Supporting information

Exploring the Potential of Two-Dimensional Bismuth–Copper Hybrid Double Perovskites for Memristor Applications

Mohamed Saber Lassoued +[a], Wang Kun+[b], Faizan Ahmad [b], Bai Sun* [b] and Yan-Zhen Zheng*[a] [b]

[+] contributed equally to this work

[a] Dr. Mohamed Saber Lassoued, and Prof. Yan-Zhen Zheng

School of Chemistry, Xi'an Jiaotong University, 99 Yanxiang Road, Xi'an, Shaanxi 710054, P R. China.State Key Laboratory of Electrical Insulation and Power Equipment, Xi'an Key Laboratory of Electronic Devices and Materials Chemistry, Xi'an Jiaotong University, Xi'an 710054, China

E-mail: zheng.yanzhen@xjtu.edu.cn

[b] Mr. Wang Kun, Mr. Faizan Ahmad, Prof. Bai Sun, and Prof. Yan-Zhen Zheng

Frontiers Institute of Technology, Xi'an Jiaotong University, 99 Yanxiang Road, Xi'an, Shaanxi 710054, P R. China, Xi'an Jiaotong University, Xi'an 710054, China

E-mail: baisun@xjtu.edu.cn

CONTENTS

1. General remarks

Single-crystal X-ray diffraction (SC-XRD) data for the $(H_2MPP)_2BiCuI_8$ was collected at 298 K using a Bruker SMART APEX II CCD diffractometer equipped with graphite-monochromated Mo-Kα radiation ($\lambda = 0.71073$ Å) and the θ–ω scan mode. Powder X-ray diffraction (PXRD) measurements were performed under ambient conditions (298 K) on a Rigaku D/max-IIIA diffractometer with Cu-Kα radiation ($\lambda = 1.54056$ Å). The crystalline powder samples were obtained by grinding the single crystals and scanned in the 2θ range of 5°–50° at a rate of 10°/min. Solid-state UV–Vis diffuse reflectance spectra were recorded on a SHIMADZU UV-3600 UV–Vis–NIR spectrophotometer, using $BaSO_4$ powder as the reflectance standard. The current-voltage (I-V) characteristics of the devices were evaluated using an electrochemical workstation equipped with a Keysight B2900 source meter and a probe station. All density-functional theory (DFT) calculations were conducted using the CASTEP module in Materials Studio 2019.

2. Characterization methods and Simulation details

2.1. Characterization methods

X-ray Crystallographic Study

Single-crystal X-ray diffraction data for **$(H_2MPP)_2BiCuI_8$** sample was were collected at 298 K using a Bruker SMART APEX II CCD diffractometer equipped with Mo Kα radiation ($\lambda = 0.71073$ Å) and the θ–ω scan mode. The resulting structures were solved by direct methods and refined through full-matrix least-squares procedures implemented in the SHELXTL program suite,[S1] with all non-hydrogen atoms refined anisotropically. Powder X-ray diffraction (PXRD) intensities were obtained at room temperature (298 K) using a Rigaku D/max-IIIA diffractometer and Cu Kα radiation ($\lambda = 1.54056$ Å). Detailed crystallographic data are summarized in **Tables S1–S4**. The CCDC numbers for **$(H_2MPP)_2BiCuI_8$** is 2412890. These crystallographic data are available in the Supporting Information or can be accessed free of charge through the Inorganic Crystal Structure Database via http://www.ccdc.cam.ac.uk/data_request/cif.

Powder XRD: The crystalline powder samples, obtained by finely grinding single-crystals, were measured at room temperature over a 2θ range of 5°–50° with a scanning rate of 5°/min.

Morphological and elemental analyses were carried out using a KYKY-EM3200 scanning electron microscope (SEM) operating at 25 kV, coupled with an Oxford X-MaxN energy-dispersive X-ray spectrometer (EDS).

Optical measurements were conducted by recording solid-state UV–Vis diffuse reflectance spectra of both pressed powder and film samples on a SHIMADZU UV-3600 UV–Vis–NIR spectrophotometer, with $BaSO_4$ powder serving as the reflectance reference.

Thermogravimetric analysis (TGA) was performed using a METTLER TOLEDO TGA/DSC3+ Extreme instrument. Samples were heated from room temperature to 700 K at a rate of 10 K/min under a nitrogen atmosphere to assess their thermal stability.

The current-voltage (I-V) characteristics of the devices were evaluated using an electrochemical workstation outfitted with a Keysight B2900 source meter (Beijing, China) and a probe station from XIBI Semiconductor Technology Co., Ltd (Shanghai, China).

2.2 Simulation Details and Computational Methods: All simulations in this study were performed using density functional theory (DFT), [S2, S3] as implemented in the BIOVIA Materials Studio Simulation Package. We employed the generalized gradient approximation (GGA) with the Perdew−Burke−Ernzerhof (PBE) functional for the electronic structure calculations. [S4, S5] The self-consistent field convergence threshold was set to 2×10^{-6} eV/atom. We utilized an OTFG norm-conserving pseudopotential with an energy cutoff of 1224.50 eV. Band structure calculations and Partial DOS for $(H_2MPP)_2BiCuI_8$ were conducted without spin-orbit coupling (SOC).

2.3. Experimental Section

Materials

Bismuth iodide (BiI$_3$), Copper iodide (CuI), 1-methylpiperidine-4-amine, Potassuim iodide (KI) and hydroiodic acid (55 wt % in H$_2$O) were purchased by Sigma Aldrich chemicals.

2.3.1. Syntheses of (H$_2$MPP)$_2$BiCuI$_8$ single crystals
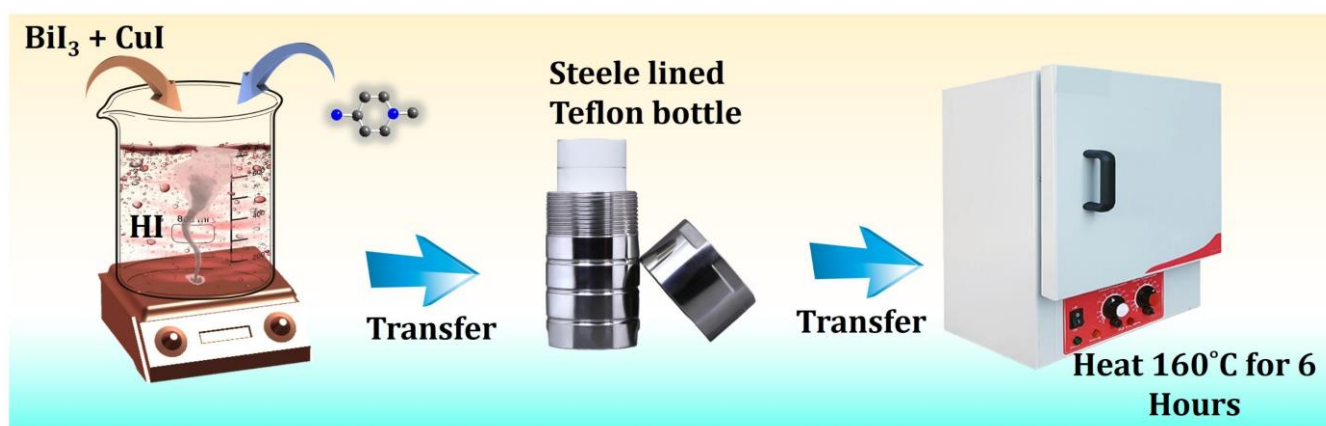
(H$_2$MPP)$_2$BiCuI$_8$ was synthesized by combining BiI$_3$ (0.5 mmol), CuI (1 mmol), 1-methylpiperidine-4-amine (2 mmol), and concentrated HI acid (5 ml) into a slurry. This mixture was heated at 160 °C for 6 hours within a PTFE-lined reaction kettle. Subsequently, single crystals of the compound were obtained through a controlled cooling process to room temperature over 24 hours. The resulting single crystals display a reddish-black opaque appearance and are plate-like in shape. These crystals were then washed with ethanol and dried under vacuum, achieving a yield of approximately 83% based on bismuth.

2.3.2. Fabrication of (H$_2$MPP)$_2$BiCuI$_8$ Memristor:

Crystals (0.5 g) produced via solvothermal reactions were dissolved in 1 ml of anhydrous DMF to create black solutions that exhibited no Tyndall effect. Both ITO-coated and ordinary glass slides were cleaned using detergent, followed by sequential ultrasonic bathing in deionized water, acetone, and isopropyl alcohol for 15 minutes each. Subsequently, the slides underwent ultraviolet ozone treatment for 30 minutes. The solutions were then spin-coated onto the slides at 2000 rpm for 60 seconds, accelerating at

1000 rpm/s. After spin-coating, the films were annealed on a hot plate at 70 °C for 10 minutes, during which they exhibited a noticeable color transition from light yellow to dark red. Finally, the device fabrication was completed by depositing Ag as the top electrode via magnetic sputtering using a metal mask.

2.4. Bond length distortion

The distortion index Δd of the $[BiI_6]$ and $[CuI_6]$ octahedra can be quantitatively calculated using the following equation:

$$\Delta d = \left(\frac{1}{n}\right) \sum_{i=1}^{n} \left(\frac{d_i - d}{d}\right)^2$$

where d refers the average distance of M–I (M=Bi, Cu) bonds and di is the individual bond length of M–I (M=Bi, Cu). The calculated distortion parameters indicate that the $[CuI_6]$ octahedra exhibit a greater degree of distortion compared to the $[BiI_6]$ octahedra (**Table S4**).

2.5. Hirshfeld surface (HS) analysis was employed to investigate the hydrogen bond interactions crucial to the nucleation and growth of crystals, specifically those involving the inorganic cores of bismuth/silver iodide units and the surrounding organic ligands (**Fig. S2**). This analysis uses parameters such as di and de—the distances from the Hirshfeld surface to the nearest internal and external atomic nuclei, respectively—to calculate a normalized contact distance (d_{norm}), which aids in the generation of HS maps. These maps show interactions with red areas indicating non-covalent interactions shorter than the van der Waals radii, white areas representing equal distances, and blue areas for interactions longer than these radii (**Fig. S2a**). In addition to the **d_norm** map, further insights into the nature of the interactions can be obtained as well from the **di** map (**Fig. S2b**), **Shape Index** (**Fig. S2c**) and **curvedness** (**Fig. S2d**).

Significant insights were gleaned from the HS maps and two-dimensional fingerprint plots, which highlighted the prevalence of hydrogen bonds, specifically H···I and H···H, marked by red spots indicating their critical role in the compound's molecular architecture (**Fig. S2e**). Interestingly, hydrogen bonding

was found to be the dominant interaction, accounting for 58.6% (H···I) and 22.5% (H···H) of the crystal packing in **(H₂MPP)₂BiCuI₈** (**Fig. S2f**).

Additionally, the analysis extended to examining bond lengths and angles within these structures to evaluate their ability to induce lattice distortions conducive to singlet excited states. Our findings indicate a greater propensity for bond length distortions within the $[CuI_6]^{2-}$ octahedral compared to $[BiI_6]^{2-}$ counterpart, suggesting enhanced flexibility and interactive potential. The lattice structure of **(H₂MPP)₂BiCuI₈** showed a crystal void volume and surface area (Void volume: 295.50 Å^3, Surface area: 811.37 Å^2), which may contribute to its unique electronic properties and potential applications in optoelectronic devices (**Fig.S2g**).

1. Supporting Tables

Table S1. Crystal data and structure refinement for **(H$_2$MPP)$_2$BiCuI$_8$**.

Compound	(H$_2$MPP)$_2$BiCuI$_8$
Empirical formula	C$_{12}$ H$_{32}$ Bi Cu I$_8$ N$_4$
Formula weight	1520.15
Crystal dimensions (mm)	0.10*0.20*0.18
Crystal system	Monoclinic
Space group	$C2$
a/Å	55.59 (3)
b/Å	10.170 (5)
c/Å	8.432 (4)
α/°	90
β/°	91.801
γ/°	90
Volume/Å3	4765 (4)
Z	6
ρ calcg/cm3	3.179
μ /mm-1	13.54
F(000)	4008
h, k, l max	69,12,10
Data Completeness	100.00%
Data/restraints/parameters	3674/132/0
Goodness-of-fit on F^2	1.05
Weight	w = 1/[σ2(F$_\circ$ ^{2}) + (0.0483P)^2 + 443.3602P] where P = (F$_\circ$ ^{2} + 2F$_c$ ^{2})/3
R-factors	R[F^2 > 2σ(F2)] = 0.056, wR(F^2) = 0.155
CCDC Number	2412890

Table S2. Summary of selected bond lengths (Å) and bond angles (°) of **(H₂MPP)₂BiCuI₈**

Bonds	Length /Å	Bonds	Length /Å	Bonds	Length /Å
Bi1—I11	3.098 (3)	C9—H9A	0.9700	I7—Bi2—I8	88.71 (8)
Bi1—I11ⁱ	3.098 (3)	C9—H9B	0.9700	I7—Bi2—I5	90.73 (8)
Bi1—I004ⁱⁱ	3.103 (3)	C9—C8	1.50 (6)	I7—Bi2—I3ᵛ	177.95 (9)
Bi1—I004ⁱⁱⁱ	3.103 (3)	N5—H5A	0.8900	I7—Bi2—I2ᵛⁱ	90.07 (8)
Bi1—I10	3.044 (3)	N5—H5B	0.8900	I5—Bi2—I8	179.16 (9)
Bi1—I10ⁱ	3.044 (3)	N5—H5C	0.8900	I3ᵛ—Bi2—I8	90.54 (8)
Bi2—I006ⁱᵛ	3.068 (3)	N5—C7	1.48 (4)	I3ᵛ—Bi2—I5	90.04 (8)
Bi2—I7	3.046 (3)	C8—H8A	0.9700	I3ᵛ—Bi2—I2ᵛⁱ	88.02 (9)
Bi2—I8	3.097 (3)	C8—H8B	0.9700	I2ᵛⁱ—Bi2—I8	88.96 (8)
Bi2—I5	3.095 (3)	C8—C7	1.53 (6)	I2ᵛⁱ—Bi2—I5	91.67 (8)
Bi2—I3ᵛ	3.084 (3)	C2—H2D	0.9700	Cu2—I10—Bi1	169.68 (10)
Bi2—I2ᵛⁱ	3.090 (3)	C2—H2E	0.9700	Cu1—I3—Bi2ⁱⁱⁱ	166.22 (13)
I9—Cu2	2.532 (5)	C16—H16A	0.9700	Cu1—I2—Bi2ᵛⁱⁱ	172.29 (13)
I10—Cu2	2.981 (10)	C16—H16B	0.9700	I9ᵛⁱⁱⁱ—Cu2—I9	139.9 (6)
I4—Cu1	2.486 (5)	C5—H5D	0.9700	I9—Cu2—I10	108.46 (18)
I1—Cu1	2.495 (5)	C5—H5E	0.9700	I9—Cu2—I10ᵛⁱⁱⁱ	100.78 (17)
I3—Cu1	2.964 (6)	C5—C4	1.54 (4)	I9ᵛⁱⁱⁱ—Cu2—I10ᵛⁱⁱⁱ	108.46 (18)
I2—Cu1	2.936 (6)	N3—H3	0.9800	I9ᵛⁱⁱⁱ—Cu2—I10	100.78 (17)
N6—H6	0.9800	N3—C6	1.45 (4)	I10—Cu2—I10ᵛⁱⁱⁱ	85.5 (4)
N6—C10	1.52 (4)	N3—C4	1.50 (4)	I4—Cu1—I1	144.1 (3)
N6—C12	1.50 (4)	C18—H18A	0.9600	I4—Cu1—I3	96.70 (16)
N6—C9	1.56 (5)	C18—H18B	0.9600	I4—Cu1—I2	105.25 (16)
N2—H2A	0.8900	C18—H18C	0.9600	I1—Cu1—I3	108.50 (17)
N2—H2B	0.8900	C7—H7	0.9800	I1—Cu1—I2	99.43 (16)
N2—H2C	0.8900	C6—H6A	0.9600	I2—Cu1—I3	91.23 (19)
N2—C14	1.62 (5)	C6—H6B	0.9600	C13—N1—C18	113 (3)
C15—H15A	0.9700	C11—H11A	0.9700	C16—N1—H1	107.5
C15—H15B	0.9700	C11—H11B	0.9700	C18—N1—H1	107.5
C15—C14	1.49 (6)	C11—C7	1.47 (5)	C18—N1—C16	108 (3)
C15—C16	1.43 (6)	C1—H1A	0.9800	N6—C12—H12A	109.5
C14—H14	0.9800	C1—C2	1.52 (5)	N6—C12—H12B	109.5
C14—C17	1.42 (6)	C1—C5	1.44 (4)	N6—C12—H12C	109.5
C10—H10A	0.9700	C6—H6C	0.9600	H12A—C12—H12B	109.5
C10—H10B	0.9700	C4—H4A	0.9700	H12A—C12—H12C	109.5
C10—C11	1.52 (4)	C4—H4B	0.9700	H12B—C12—H12C	109.5
C13—H13A	0.9700	N4—H4C	0.8900	H3A—C3—H3B	107.1
C13—H13B	0.9700	N4—H4D	0.8900	C2—C3—H3A	107.7
C13—N1	1.46 (5)	N4—H4E	0.8900	C2—C3—H3B	107.7
C13—C17	1.54 (5)	I11—Bi1—I11ⁱ	179.25 (10)	C2—C3—N3	118 (4)
C1—N4	1.48 (6)	I11ⁱ—Bi1—I004ⁱⁱ	90.55 (7)	N3—C3—H3A	107.7
N1—H1	0.9800	I11—Bi1—I004ⁱⁱ	89.99 (7)	N3—C3—H3B	107.7
N1—C16	1.54 (6)	I11—Bi1—I004ⁱⁱⁱ	90.55 (7)	C14—C17—C13	103 (3)
N1—C18	1.50 (4)	I11ⁱ—Bi1—I004ⁱⁱⁱ	89.99 (7)	C14—C17—H17A	111.1
C12—H12A	0.9600	I004ⁱⁱⁱ—Bi1—I004ⁱⁱ	86.67 (11)	C14—C17—H17B	111.1
C12—H12B	0.9600	I10—Bi1—I11	88.17 (7)	C13—C17—H17A	111.1
C12—H12C	0.9600	I10—Bi1—I11ⁱ	91.32 (7)	H17A—C17—H17B	109.1
C3—H3A	0.9700	I10ⁱ—Bi1—I11ⁱ	88.17 (7)	N6—C9—H9A	109.5
C3—H3B	0.9700	I10ⁱ—Bi1—I11	91.32 (7)	N6—C9—H9B	109.5
C3—C2	1.44 (6)	I006ⁱᵛ—Bi2—I5	87.98 (8)	H9A—C9—H9B	108.1
C3—N3	1.59 (5)	I006ⁱᵛ—Bi2—I3ᵛ	90.01 (8)	C8—C9—N6	111 (3)
C17—H17A	0.9700	I006ⁱᵛ—Bi2—I2ᵛⁱ	178.00 (9)	C8—C9—H9A	109.5
C17—H17B	0.9700	I7—Bi2—I006ⁱᵛ	91.91 (9)	H17A—C17—H17B	109.1

.

Bonds	Length /Å	Bonds	Length /Å	Bonds	Length /Å
C8—C9—H9B	109.5	C11—C10—H10A	109.7	H18A—C18—H18C	109.5
H5A—N5—H5B	109.5	C11—C10—H10B	109.7	H18B—C18—H18C	109.5
H5A—N5—H5C	109.5	H13A—C13—H13B	108.2	C11—C7—N5	115 (3)
H5B—N5—H5C	109.5	N1—C13—H13A	109.8	C11—C7—C8	109 (3)
C7—N5—H5A	109.5	N1—C13—H13B	109.8	C11—C7—H7	107.9
C7—N5—H5B	109.5	N1—C13—C17	109 (3)	N5—C7—C8	109 (3)
C7—N5—H5C	109.5	C17—C13—H13A	109.8	N5—C7—H7	107.9
C9—C8—H8A	108.9	C17—C13—H13B	109.8	C8—C7—H7	107.9
C9—C8—H8B	108.9	C10—C11—H11A	109.3	N3—C6—H6A	109.5
C9—C8—C7	113 (4)	C10—C11—H11B	109.3	N3—C6—H6B	109.5
H8A—C8—H8B	107.7	H11A—C11—H11B	107.9	N3—C6—H6C	109.5
C7—C8—H8A	108.9	C7—C11—C10	112 (3)	H6A—C6—H6B	109.5
C7—C8—H8B	108.9	C7—C11—H11A	109.3	H6A—C6—H6C	109.5
C1—C2—H2D	109.6	C7—C11—H11B	109.3	H6B—C6—H6C	109.5
C1—C2—H2E	109.6	C2—C1—H1A	107.3	C5—C4—H4A	109.3
C3—C2—C1	110 (4)	C5—C1—H1A	107.3	C5—C4—H4B	109.3
C3—C2—H2D	109.6	C5—C1—C2	111 (3)	N3—C4—C5	112 (2)
C3—C2—H2E	109.6	C5—C1—N4	115 (4)	N3—C4—H4A	109.3
C10—N6—H6	107.0	N4—C1—H1A	107.3	N3—C4—H4B	109.3
C10—N6—C9	109 (3)	N4—C1—C2	109 (3)	H4A—C4—H4B	107.9
C12—N6—H6	107.0	C13—N1—H1	107.5	C1—N4—H4C	109.5
C12—N6—C10	113 (3)	C13—N1—C16	114 (3)	C1—N4—H4D	109.5
C12—N6—C9	114 (3)	N6—C10—C11—C7	63 (3)	C1—N4—H4E	109.5
C9—N6—H6	107.0	H2D—C2—H2E	108.1	H4C—N4—H4D	109.5
H2A—N2—H2B	109.5	C15—C16—N1	112 (3)	H4C—N4—H4E	109.5
H2A—N2—H2C	109.5	C15—C16—H16A	109.3	H4D—N4—H4E	109.5
H2B—N2—H2C	109.5	C15—C16—H16B	109.3		
C14—N2—H2A	109.5	N1—C16—H16A	109.3		
C14—N2—H2B	109.5	N1—C16—H16B	109.3		
C14—N2—H2C	109.5	H16A—C16—H16B	108.0		
H15A—C15—H15B	108.2	C1—C5—H5D	109.3		
C14—C15—H15A	109.8	C1—C5—H5E	109.3		
C14—C15—H15B	109.8	C1—C5—C4	112 (3)		
C16—C15—H15A	109.8	H5D—C5—H5E	107.9		
C16—C15—H15B	109.8	C4—C5—H5D	109.3		
C16—C15—C14	109 (4)	C4—C5—H5E	109.3		
N2—C14—H14	107.3	C3—N3—H3	108.1		
C15—C14—N2	106 (4)	C6—N3—C3	115 (3)		
C15—C14—H14	107.3	C6—N3—H3	108.1		
C17—C14—N2	107 (4)	C6—N3—C4	111 (3)		
C17—C14—C15	122 (4)	C4—N3—C3	106 (2)		
C17—C14—H14	107.3	C4—N3—H3	108.1		
N6—C10—H10A	109.7	N1—C18—H18A	109.5		
N6—C10—H10B	109.7	N1—C18—H18B	109.5		
N6—C10—C11	110 (3)	N1—C18—H18C	109.5		
H10A—C10—H10B	108.2	H18A—C18—H18B	109.5		

Symmetry codes: (i) −x+1, y, −z+1; (ii) −x+1, y+1, −z; (iii) x, y+1, z+1; (iv) x, y, z−1; (v) x, y−1, z−1; (vi) x, y−1, z; (vii) x, y, z+1; (viii) x, y+1, z; (ix)−x+1, y, −z.

Table S3. Bond lengths (di) and bond distortions (Δd) for **(H₂MPP)₂BiCuI₈** compound.

(H₂MPP)₂BiCuI₈							
[BiI$_6$] Octahedral	**d=3.079Å**	**Individual bond lengths (di)**					
		3.045 Å	**3.096 Å**	**3.067 Å**	**3.084 Å**	**3.094 Å**	**3.090 Å**
Bond length Distortion (Δd)		1.2×10^{-4}	3.0×10^{-5}	1.0×10^{-4}	2.63×10^{-6}	2.0×10^{-5}	1.0×10^{-5}
[CuI$_6$] Octahedral	**d = 3.029 Å**	**3.096 Å**	**2.486 Å**	**2.935 Å**	**2.494 Å**	**4.229 Å**	**2.934 Å**
		1.5×10^{-2}	9.3×10^{-3}	4.4×10^{-3}	8.7×10^{-3}	8.92×10^{-2}	4.4×10^{-3}

Table S4. Potential hydrogen bonding data of compound **(H₂MPP)₂BiCuI₈**

D-H	d(D-H)	d(H..A)	<DHA	d(D..A)	A
N6-H6	0.98	2.506	175.93	3.484	I9
N2-H2A	0.89	2.728	160.17	3.578	I4
N2-H2B	0.89	2.848	148.33	3.635	I11 [x, y-1, z]
N2-H2C	0.89	2.979	148.22	3.765	I10 [x, y-1, z]
N2-H2C	0.89	3.18	125.02	3.762	I10 [-x+1, y-1, -z]
C14-H14	0.98	3.104	161.98	4.047	I11 [x, y-1, z-1]
C10-H10A	0.97	3.092	141.32	3.896	I11 [x, y-1, z]
C13-H13A	0.97	3.136	157.2	4.048	I8
C1-H1A	0.98	2.476	178.57	3.455	I1
N1-H1	0.98	2.516	177.77	3.495	I4
C12-H12B	0.96	3.153	132.06	3.863	I10 [-x+1, y, -z+1]
C17-H17A	0.97	3.294	146.34	4.137	I9 [x, y-1, z]
C9-H9A	0.97	3.134	150.42	4.006	I11
N5-H5A	0.89	2.949	148.63	3.738	I6 [x, y+1, z]
N5-H5A	0.89	3.167	127.22	3.773	I7 [x, y+1, z]
N5-H5B	0.89	2.76	178.68	3.65	I8 [x, y+1, z]
N5-H5C	0.89	2.863	136.48	3.561	I3
N5-H5C	0.89	3.039	121.58	3.586	I2
C8-H8A	0.97	3.256	147.25	4.106	I4 [x, y+1, z]
C2-H2D	0.97	3.029	146.22	3.873	I5 [x, y+1, z+1]
C16-H16A	0.97	3.114	134.08	3.852	I8 [x, y+1, z]
C5-H5D	0.97	3.187	145.54	4.024	I5 [x, y, z+1]
N3-H3	0.98	3.145	158.43	4.072	I5 [-x+3/2, y+1/2, -z+1]
C18-H18C	0.96	3.31	171.71	4.262	I4 [x, y, z-1]
C7-H7	0.98	3.149	162.74	4.095	I8 [x, y+1, z+1]
C6-H6A	0.96	2.703	165.96	3.642	I5 [-x+3/2, y+1/2, -z]
C6-H6B	0.96	3.006	126.7	3.662	I3 [-x+3/2, y-1/2, -z+1]
C6-H6B	0.96	2.976	125.37	3.617	I2 [-x+3/2, y-1/2, -z+1]
C6-H6C	0.96	3.107	120.04	3.682	I6 [-x+3/2, y+1/2, -z]
C6-H6C	0.96	2.814	150.91	3.683	I7 [-x+3/2, y+1/2, -z+1]
C4-H4A	0.97	3.284	156.78	4.193	I1 [-x+3/2, y-1/2, -z+1]
N4-H4C	0.89	3.263	147.87	4.045	I3
N4-H4D	0.89	3.118	141.14	3.852	I2 [x, y, z+1]
N4-H4E	0.89	3.216	162.44	4.074	I7 [x, y, z+1]

Table S5. Stability tests and band gap comparison of **$(H_2MPP)_2BiCuI_8$** with other reported lead-free halide perovskite materials.

Compounds	Stability Test period (days)	Test condition	Band gap (eV)	Ref.
[(3AMPY)$_2$AgBiI$_8$·H$_2$O]	30	55% RH	1.86	[S6]
(DPA)$_4$AgBiBr$_8$	-	-	2.44	[S7]
(C$_6$H$_{16}$N$_2$)$_2$AgBiI$_8$·H$_2$O	30	55% RH	1.93	[S8]
(C$_6$H$_{16}$N$_2$)$_2$CuBiI$_8$·0.5H$_2$O	30	55% RH	1.68	[S8]
(C$_6$H$_{16}$N$_2$)$_2$BiAgI$_8$.H$_2$O	30	55% RH	2	[S9]
(NH$_3$C$_5$H$_9$)$_4$AgSbI$_8$	60	55% RH	2.37	[S10]
(NH$_3$C$_8$H$_{15}$)$_4$AgSbI$_8$	60	55% RH	2.44	[S10]
(NH$_3$C$_6$H$_{11}$)$_4$AgSbI$_8$	60	55% RH	2.39	[S10]
(H$_2$MPP)$_2$BiCuI$_8$	**90**	**55% RH**	**1.65**	**This work**

3AMPY = 3-(aminomethyl) pyridinium)/ DPA = 2,2-dimethylpropan-1-aminium/ H$_2$MPP = 1-methylpiperidinium-4-amine
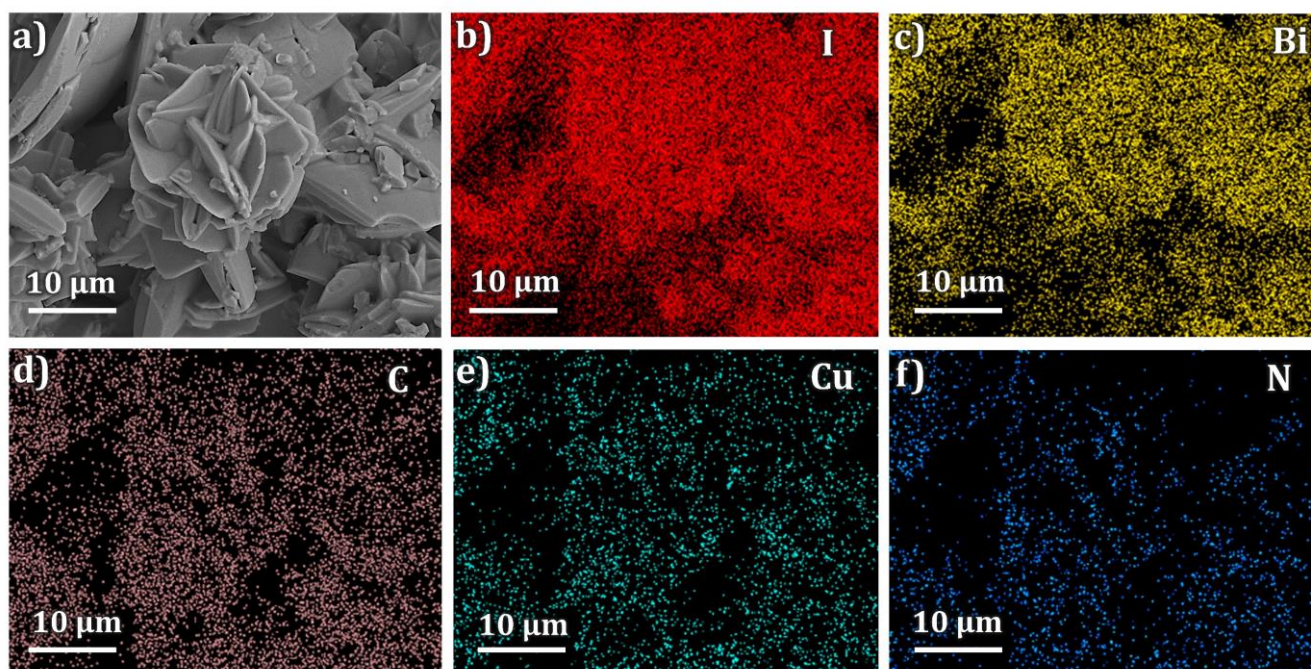
Figure S1. (a) **(H₂MPP)₂BiCuI₈** sample SEM and (b-f) elemental mapping of I, Bi, C, Cu and N for a single crystal
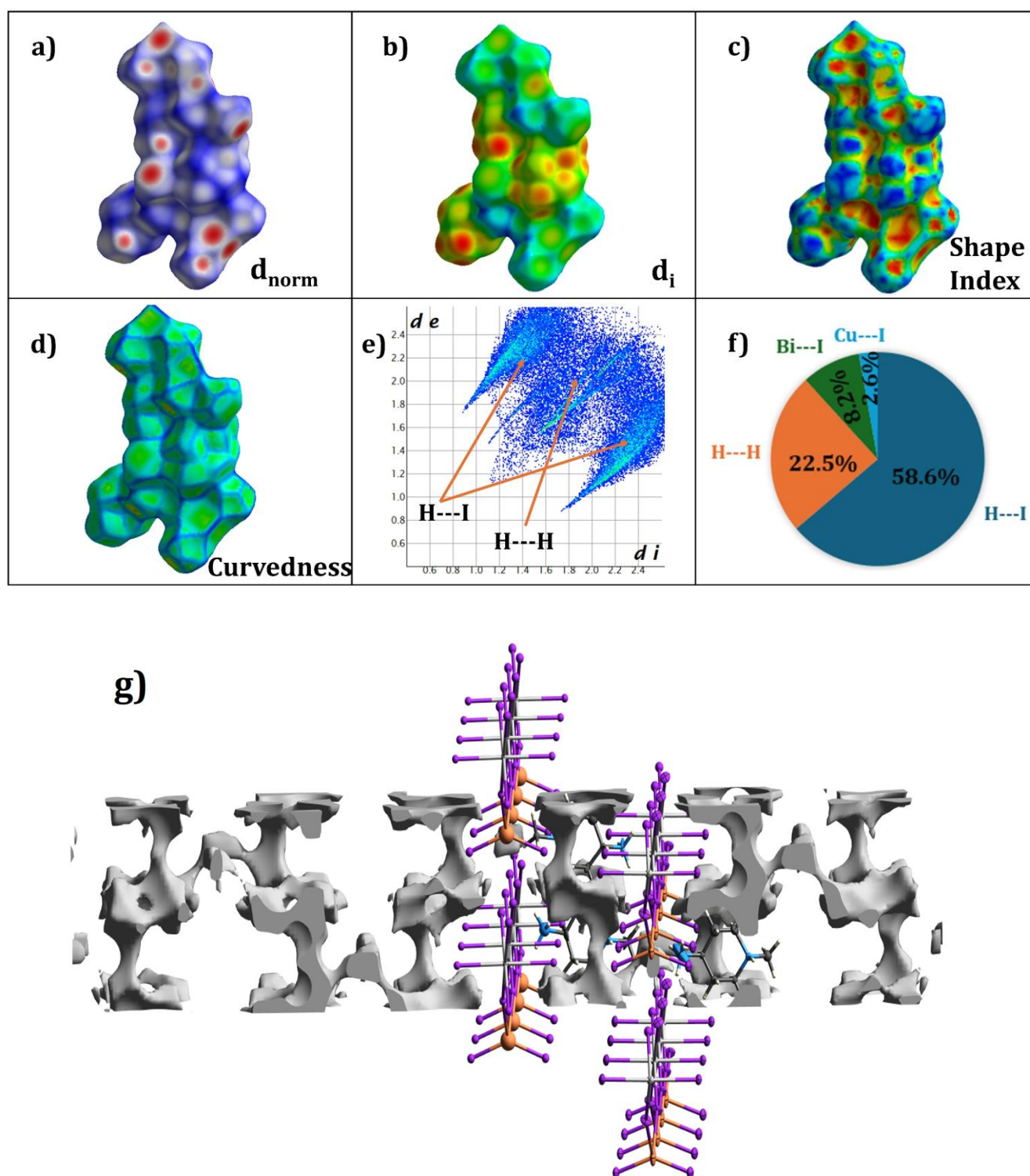
Figure S2. (a-d) Hirshfeld surfaces mapped with d_{norm} (a), di (b), Shape index (c) and curvedness (d) for **(H₂MPP)₂BiCuI₈**; (e) two-dimensional finger prints plots for **(H₂MPP)₂BiCuI₈**; (f) Interatomic and intra-atomic interactions for **(H₂MPP)₂BiCuI₈**; (g) voids analysis for **(H₂MPP)₂BiCuI₈**

	C	N	Bi	Cu	I
Exp(%)	9.01	3.12	12.79	3.68	71.4
Theo(%)	9.24	3.68	13.74	4.18	66.78
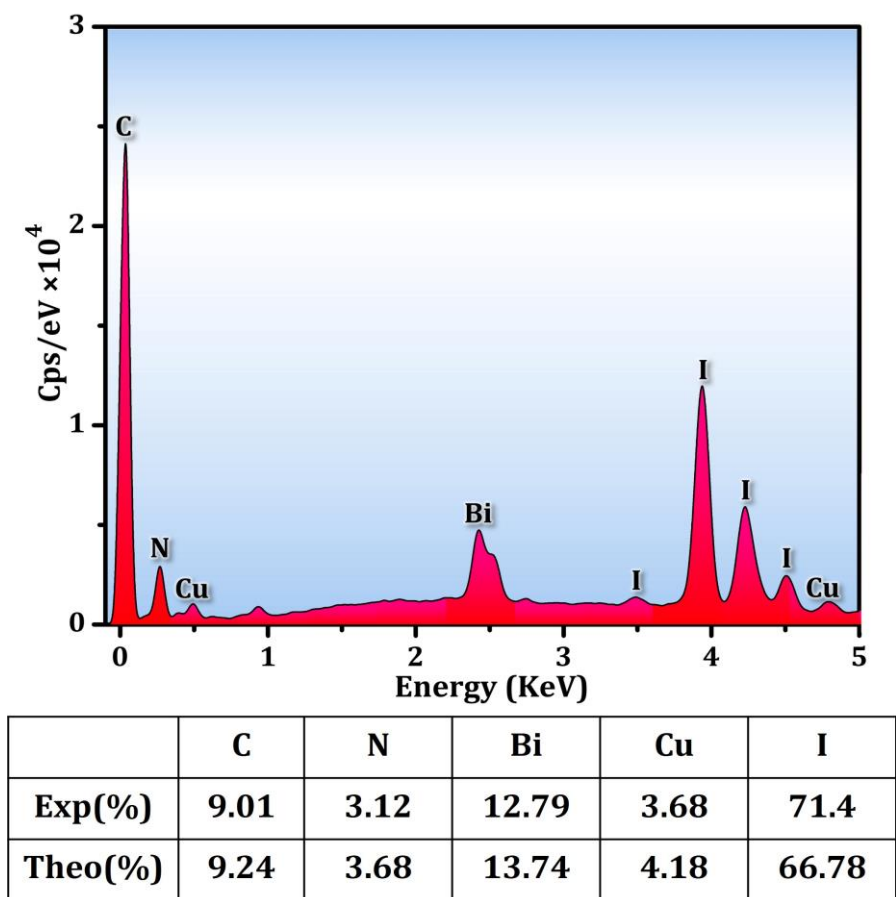
Figure S3. Elemental analysis result for C, N, Bi, Cu and I in **(H₂MPP)₂BiCuI₈**
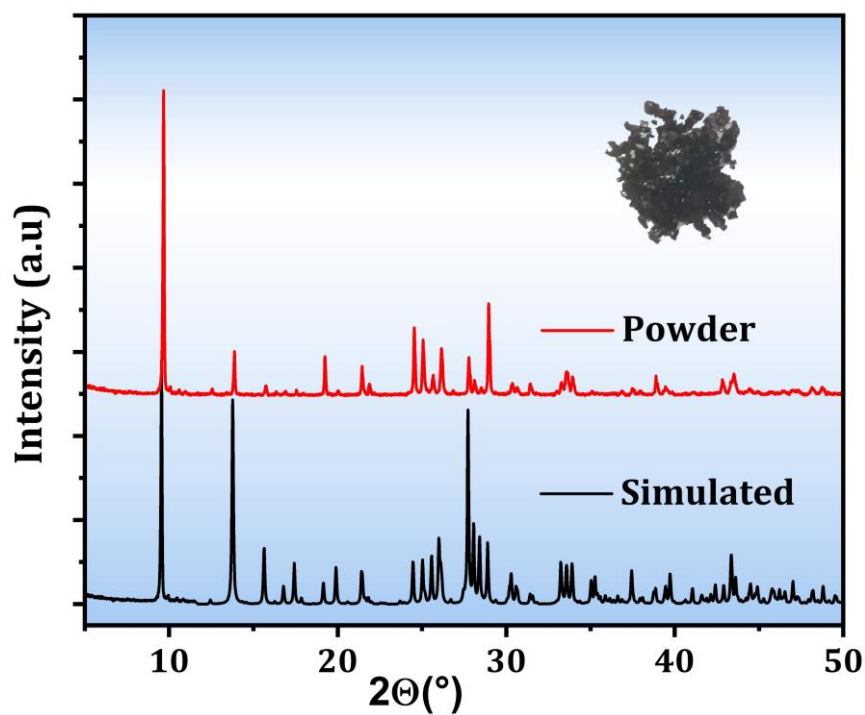
Figure S4. The experimental PXRD pattern of **(H₂MPP)₂BiCuI₈** in comparison to its simulation pattern
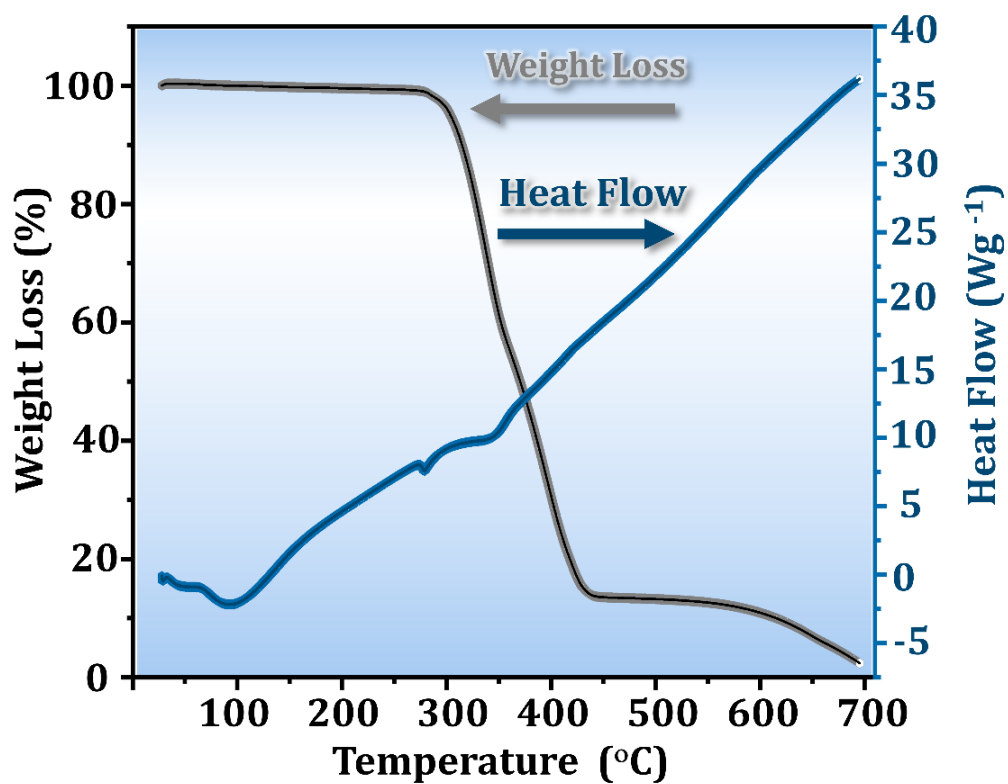
Figure S5. TGA curves of **(H₂MPP)₂BiCuI₈**
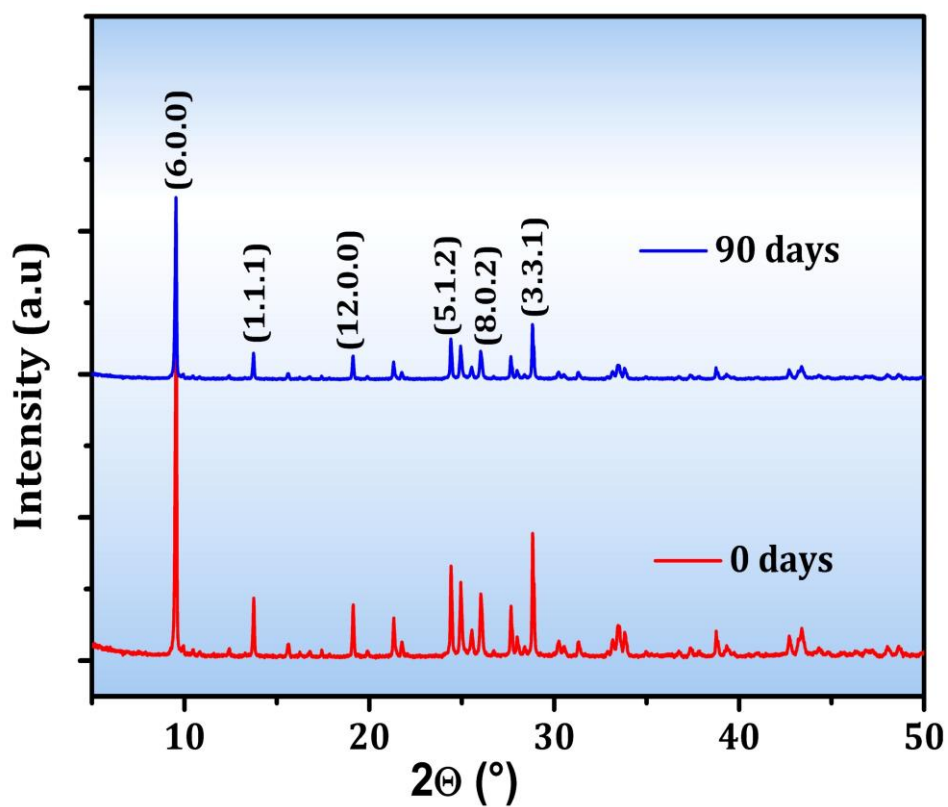
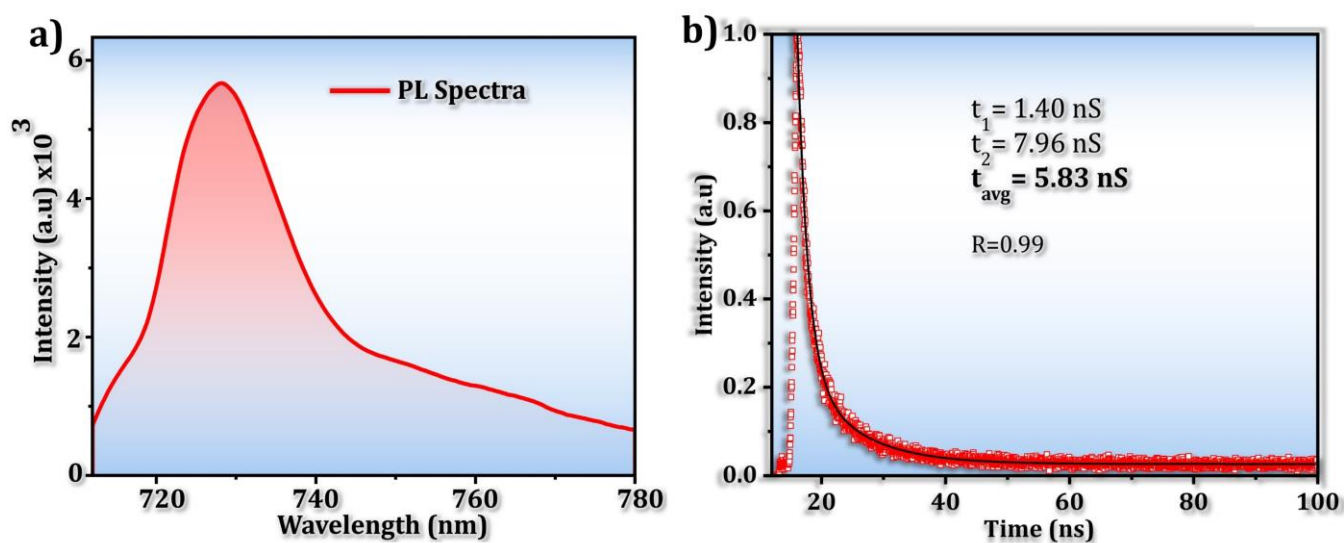**Figure S6**. XRD patterns of **(H₂MPP)₂BiCuI₈** powder before and after exposure to humidity (55% RH) for 90 days

Figure S7. (a) The steady-state room-temperature photoluminescence (PL) spectra of $(H_2MPP)_2BiCuI_8$. (b) Time-resolved PL decay profile of $(H_2MPP)_2BiCuI_8$ fitted with a bi-exponential model
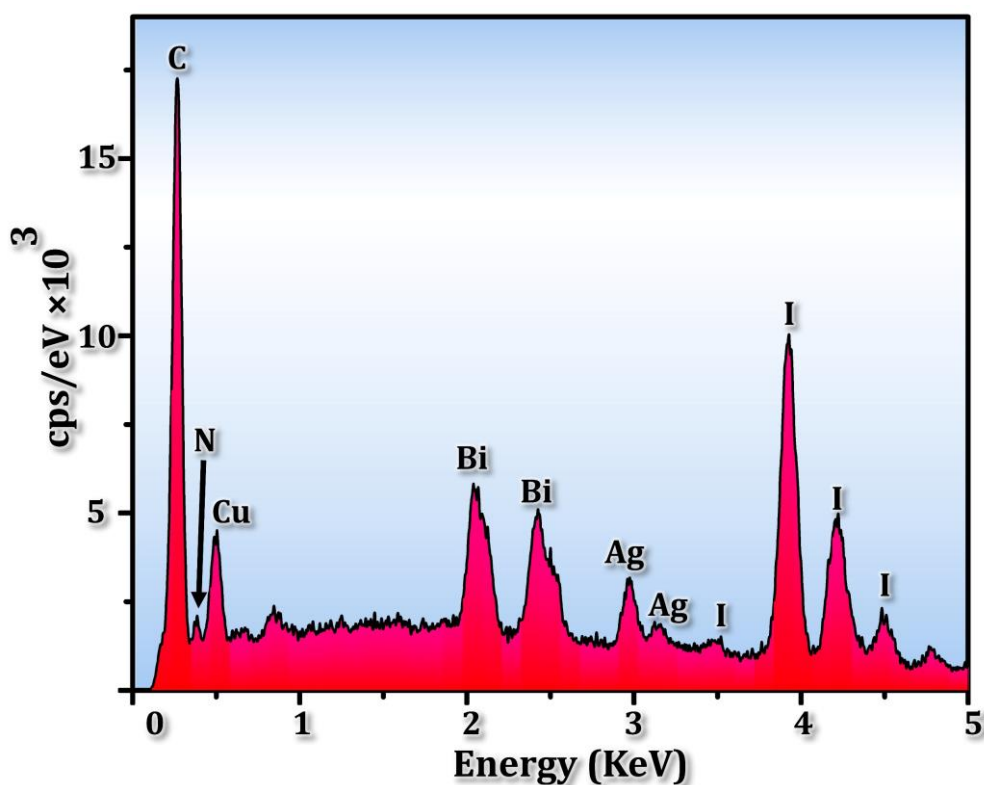

Figure S8. Elemental analysis result for C, N, Bi, Cu and I in **Ag/(H₂MPP)₂BiCuI₈/ITO**

References

[S1]   G. M. Sheldrick, *Acta Crystallogr A* **2008**, *64*, 112-122.

[S2]   J. Hafner, *Journal of Computational Chemistry* **2008**, *29*, 2044-2078.

[S3]   J. P. Perdew, K. Burke, M. Ernzerhof, *Physical Review Letters* **1996**, *77*, 3865-3868.

[S4]   D. M. Ceperley, B. J. Alder, *Physical Review Letters* **1980**, *45*, 566-569.

[S5]   J. P. Perdew, A. Zunger, *Physical Review B* **1981**, *23*, 5048-5079.

[S6]   D. Fu, S. Wu, Y. Liu, Y. Yao, Y. Hea and X-M. Zhang, Inorg. Chem. Front., 2021,8, 3576-3580.

[S7]   C-Y. Su, Y-F. Yao, Z-X. Zhang, Y. Wang, M. Chen, P-Z. Huang, Y. Zhang, W-C. Qiao and D-W. Fu, Chem. Sci. , 2022,13, 4794-4800.

[S8]   L-Y. Bi, Y-Q. Hu, M-Q. Li, T-L. Hu, H-L. Zhang, X-T. Yin, W-X. Que, M. S. Lassoued and Y-Z. Zheng, J. Mater. Chem. A. 2019, 7, 19662-19667.

[S9]   M. S. Lassoued, L.-Y. Bi, Z. Wu, G. Zhou and Y.-Z. Zheng, J. Mater. Chem. C. 2020, 8, 5349–5354.

[S10]   Q.-W. Li, M. S. Lassoued, W.-P. Chen, G.-Y. Gou and Y.-Z. Zheng, ACS Appl. Mater. Interfaces, 2024, 16, 5769-5778.